Spectroscopic characterization of the v2 = 3 and v2 = v4 = 1 states for 15NH3 from high resolution infrared spectra

Spectroscopic characterization of the v(2)=3 and v(2) = v(4)=1 states for (NH3)-N-15 from high resolution infrared spectra

Cane, E; Di Lonardo, G; Fusina, L; TAMASSIA, F; Predoi-Cross, A

Journal of Quantitative Spectroscopy and Radiative Transfer
Volume 250, July 2020, 106987

Spectroscopic characterization of the $v_2 = 3$ and $v_2 = v_4 = 1$ states for $^{15}NH_3$ from high resolution infrared spectra

Elisabetta Canè*[a], Gianfranco Di Lonardo[a] , Luciano Fusina[a], Filippo Tamassia[a], Adriana Predoi-Cross[b]

[a]*Dipartimento di Chimica Industriale "Toso Montanari", Università di Bologna, Viale Risorgimento 4, 40136 Bologna, Italy*

[b]*Alberta Terrestrial Imaging Centre*, *Department of Physics and Astronomy, University of Lethbridge, 4401 University Drive, Lethbridge AB, T1K 3M4, Canada*

Number of pages :27

Number of figures : 4

Number of tables : 5

Supplementary Materials: Tables S1 to S14 of assigned transitions.

*Address for proofs and correspondence:
Dr. Elisabetta Canè
Dipartimento di Chimica Industriale "Toso Montanari"
Viale Risorgimento 4
40136 Bologna
ITALY
tel: +39 051 209 3707
FAX: +39 051 209 3690
E-mail elisabetta.cane@unibo.it

Abstract

The *a*, *s* inversion levels of $v_2 = 3$ and $v_2 = v_4 = 1$ vibration states of $^{15}NH_3$ are studied from high resolution infrared spectra up to 3200 cm^{-1}. Spectra were recorded from 60 to 2000 cm^{-1} using the Bruker IFS 125 interferometer located at the Canadian Light Source and from 1900 to 3200 cm^{-1} using the Bomem DA 008 in Bologna. Transitions in $3\nu_2$ and $\nu_2 + \nu_4$, in the $3\nu_2 \leftarrow \nu_2$, $\nu_2+\nu_4 \leftarrow \nu_2$, $3\nu_2 \leftarrow 2\nu_2$, $\nu_2+\nu_4 \leftarrow 2\nu_2$, $3\nu_2 \leftarrow \nu_4$, $\nu_2+\nu_4 \leftarrow \nu_4$, and $3\nu_2 \leftrightarrow \nu_2+\nu_4$ hot bands, and the rotation-inversion transitions in $3\nu_2$ and $\nu_2+\nu_4$ have been observed. 5770 transitions with J'_{max} / K'_{max} up to 15 have been assigned, including 395 perturbation allowed ones. All transitions were fitted simultaneously on the basis of a rotation-inversion Hamiltonian which includes distortion constants up to 10^{th} power in the angular momentum and all symmetry allowed interaction parameters between and within the *a*, *s* inversion levels of $v_2 = 3$ and $v_2 = v_4 = 1$. The term values of the lower levels of transitions have been calculated using the parameters recently derived for the ground and $v_2 = 1$, 2 and $v_4 = 1$ states. The data were reproduced at experimental accuracy. The results are compared with those of $^{14}NH_3$. The experimental transitions are compared with their theoretically predicted values. The list of assignments is supplied as supplementary material. The present results noticeably improve the wavenumber line list in the HITRAN 2016 data base.

Keywords: Ammonia; $^{15}NH_3$; high resolution infrared spectrum; vibration-excited bending states.

1. Introduction

Ammonia is present in various astrophysical objects and its heavier isotopologue $^{15}NH_3$ is receiving major attention in astrophysics, particularly as a tracer of the $^{14}N/^{15}N$ ratio in the universe, known not to be constant and different from the one on Earth [1,2]. The determination of the $^{14}N/^{15}N$ ratio is useful to improve our understanding of the nitrogen fractionation process in the interstellar medium (ISM) [3-6], in Jupiter and Saturn atmospheres [7-8], in meteorites [9], and in comets [10]. The determination of the nitrogen isotopic ratio in the terrestrial atmosphere, where the natural abundance of ^{15}N is not constant because of either natural or anthropogenic enhancement [11-12], is used to study the transport of ammonia emission across landscapes [13]. The characterization of the nitrogen isotopic ratio in depositions and rain events is a complementary tool for quantifying the emission sources [14-16].

The study of the infrared (IR) spectrum of ammonia in the region at 4 μm has proved to be essential to interpret the high-quality spectra of Jupiter and Saturn atmospheres [17], where ammonia is the fourth most abundant constituent. In the 4 μm range the ammonia absorption arises from higher overtones and combination bands of the bending normal modes, i.e. involving the *a*, *s* inversion levels of the $\nu_2 = 3$ and $\nu_2 = \nu_4 = 1$ vibration states. Kleiner at al. assigned 1366 transitions of the $3\nu_2/\nu_2+\nu_4$ bands with J' up to 13 from Fourier transform infrared (FTIR) spectra recorded at 0.011 cm^{-1} unapodized resolution, analyzing both line positions and intensities [18]. Later, the $3\nu_2 \leftarrow \nu_2$ and the $\nu_2+\nu_4 \leftarrow \nu_2$ hot bands have been studied by Cottaz et al. [19]; they assigned 516 transitions up to $J = 10$ and fitted the intensities of 269 lines, with a root mean squared (RMS) percent error of 7.2. Recently, the $3\nu_2/\nu_2+\nu_4$ dyad has been re-analyzed [20]. The transitions of cold bands from [18] have been added to new assignments in the $3\nu_2 \leftarrow 2\nu_2$ and $\nu_2+\nu_4 \leftarrow \nu_4$ hot bands and to the rotation-inversion transitions in $3\nu_2$ and $\nu_2 + \nu_4$ observed in the IR and Far-IR (FIR) high resolution spectra, recorded from 50 to 2800 cm^{-1} [21]. This dataset has been further implemented with about one hundred transitions from [22] for the $3\nu_2 \leftarrow \nu_2$ hot bands. A total of 3422 transitions, 2400 of which are single, have been reproduced at experimental accuracy modeling the $3\nu_2/\nu_2+\nu_4$ dyad with the Hamiltonian described in [21].

In the case of $^{15}NH_3$, the $3\nu_2/\nu_2+\nu_4$ dyad has been analyzed in the eighties from IR spectra recorded at 0.06 cm^{-1} of resolution [23], modeling the line positions by means of a vibration-rotation-inversion Hamiltonian that takes into account the stronger interactions between and within the $\nu_2 = 1, 2, 3$, $\nu_4 = 1$ and $\nu_2 = \nu_4 = 1$ states, analogously to what was done for $^{14}NH_3$ by Urban et al. [24].

Recently, new high resolution FTIR spectra of $^{15}NH_3$ have been recorded from 60 to 2000 cm^{-1} at the Canadian Light Source (CLS), in Saskatoon, Canada. The inversion and the rotation-inversion transitions between the *a*, *s* levels of the ground state (GS), of $\nu_2 = 1, 2$ and of $\nu_4 = 1$ have been assigned and those in GS and $\nu_2 = 1$ analyzed at experimental accuracy [25]. Moreover, the vibration-rotation-inversion transitions in ν_2, $2\nu_2$, ν_4, $2\nu_2 \leftarrow \nu_2$, $\nu_4 \leftarrow \nu_2$, $2\nu_2 \leftrightarrow \nu_4$ have been analyzed together with the inversion-rotation transitions in ν_2, $2\nu_2$, and ν_4 assigned in the spectra from CLS or reported in the literature, fitting simultaneously more than 7500 data. The transitions have been reproduced at experimental accuracy using 185 spectroscopic parameters, determined with high precision by means of an effective Hamiltonian that included all symmetry allowed interactions between and within the $\nu_2 = 1, 2$ and $\nu_4 = 1$ excited states [27].

Since some features and weak absorption lines observed in the spectra recorded at the CLS [25,27] could be due to transitions reaching the $\nu_2 = 3$ and $\nu_2 = \nu_4 = 1$, new FTIR high resolution spectra from 1900 to 3200 cm^{-1} have been measured to detect and assign the transitions of the $3\nu_2$ and $\nu_2+\nu_4$ bands. The results of the analysis of the cold bands have been used to predict the transitions in the hot bands and the rotation-inversion transitions that have enough intensity to be observed in the spectra recorded at CLS. The experimental data set, comprising 5770 transitions covering 11 bands, and with J'_{max} / K'_{max} equal to 15, has been analyzed to experimental accuracy by means of an effective Hamiltonian which contains all symmetry allowed interactions between and within the *a*, *s* levels of the upper states. The spectroscopic parameters of the lower states of transitions were kept fixed to the very precise values from [27].

The aims of this study are the following: the determination of the spectroscopic parameters of $\nu_2 = 3$ and $\nu_2 = \nu_4 = 1$ with high precision from experiment; the improvement of the knowledge of the line positions for $^{15}NH_3$ at 4 μm under high resolution conditions; the identification of the hot band transitions and of the rotation-inversion transitions in $\nu_2 = 3$ and $\nu_2 = \nu_4 = 1$, which have not been reported before and, eventually,

the implementation of the $^{15}NH_3$ wavenumber line list for the HITRAN data base [28]. Finally, the comparison of the experimental line positions with the theoretically predicted values [26] is presented.

The paper is structured as follows. The experimental details and the description of the spectra are given in section 2; the assignment procedure, the theoretical model and the analysis are described in section 3; the results of the fits together with the comparison between experimental and theoretically derived line list are presented in section 4 while the conclusions are drawn in section 5.

2. Experiment and description of the spectra

The sample of $^{15}NH_3$ was supplied by Sigma–Aldrich with an isotopic purity of 99% and used without any further purification. The details of the recordings for the spectra measured at CLS from 60 to 2000 cm^{-1} are reported in [25, 27]. The estimated wavenumber uncertainty of isolated lines in the FIR region is 0.4×10^{-3} cm^{-1} and 0.6×10^{-3} cm^{-1} in the IR region.

Two absorption spectra have been recorded at room temperature in the 1900 – 3200 cm^{-1} range, using a Bomem DA 008 spectrometer in Bologna. A Globar source, KBr beam splitter and InSb detector were used. The instrument was equipped with a 0.25 m base multi pass cell, set at 6 m and 10 m, and filled at 267 Pa. The gas pressure was measured using a 0-1 Torr Baratron gauge. Some impurities were identified in the spectra, namely $^{14}NH_3$, H_2O and some partially deuterated species, $^{15}NH_2D$ and HOD. The instrumental unapodized resolution was 0.008 cm^{-1}, close to the Doppler line broadening as the Doppler full width of $^{15}NH_3$ absorption lines at room temperature is about 0.007 cm^{-1} at 2500 cm^{-1}. Absorption lines of residual H_2O and CO_2 [28] have been used for calibration. The wavenumber uncertainty of isolated lines of medium intensity is estimated 0.0006 cm^{-1}.

The survey of the $3\nu_2/\nu_2+\nu_4$ region in the $^{15}NH_3$ spectrum is shown in Figure 1. The Q branches of the $s \leftarrow a$ and $a \leftarrow s$ $3\nu_2$ parallel bands are centered at about 2369 and 2876 cm^{-1}, respectively. The weaker $s \leftarrow s$ and $a \leftarrow a$ $\nu_2 + \nu_4$ perpendicular bands appear between the overtones, centered at 2534 and 2578 cm^{-1}, respectively.

[insert Fig. 1 about here]

Figure 2 illustrates the $J = 6_K \leftarrow 7_K$ and $J = 7_K \leftarrow 8_K$ $s \leftarrow a$ transitions of the $3\nu_2 \leftarrow$ GS band. Lines are blue degraded for increasing K and the intensity alternation is evident as well as the presence of the $K = 0$ line only for J even, due to nuclear spin statistical weights.

[insert Fig. 2 about here]

Figure 3 illustrates the ${}^{p}P_K(9)$ sub-branch of the $s \leftarrow s$ $\nu_2+\nu_4 \leftarrow$ GS band whose absorption lines are blue degrading but reverse their direction for $K'' > 5$.

[insert Fig. 3 about here]

In the FIR and IR spectra recorded at CLS [25,27] numerous weak vibration-rotation-inversion transitions have been identified and assigned to: $3\nu_2 \leftarrow \nu_2$, $\nu_2+\nu_4 \leftarrow \nu_2$, $3\nu_2 \leftarrow 2\nu_2$, $\nu_2+\nu_4 \leftarrow 2\nu_2$, $3\nu_2 \leftarrow \nu_4$, $\nu_2+\nu_4 \leftarrow \nu_4$, and $3\nu_2 \leftrightarrow \nu_2+\nu_4$. In addition, the $a \leftarrow s$ inversion and rotation-inversion transitions, with selection rules $\Delta J = 0$, $\Delta K = 0$ and $\Delta J = \pm 1$, $\Delta K = 0$, respectively, are observed in $\nu_2 = 3$ being the $a - s$ energy separation very large, 508.61 cm^{-1}. In the doubly degenerate $\nu_2 = \nu_4 = 1$ state four sets of levels corresponding to the vibration angular momentum $l_4 = \pm 1$ are present. Being the $a - s$ energy separation 44.23 cm^{-1} only four branches are observed in the spectra with selection rules $\Delta l = 0$, $\Delta J = +1$, $\Delta K = 0$, $a \leftarrow s$ and $s \leftarrow a$.

3. Analysis

3.1 Assignments

The analysis started from the identification of the $3\nu_2$ and $\nu_2+\nu_4$ transitions in the newly recorded spectra, updating the results previously reported in [23] with more precise wavenumbers. The extended path length and the higher resolution of the new recordings allowed to extend the assignments to some weak absorptions, particularly at high J and K values, to identify several perturbation allowed transitions to $\nu_2 = \nu_4 = 1$, and to split lines overlapped in [23], in the limit imposed by the Doppler line broadening. The correctness of the new assignments was checked by means of the GS combination differences (GSCD) calculated using the accurate parameters from [27]. The vibration-rotation-inversion transitions of the cold

bands have been fitted simultaneously (see below) to obtain the spectroscopic parameters and the term values of the *a*, *s* levels in $v_2 = 3$ and $v_2 = v_4 = 1$. Then, the rotation-inversion-transitions between the *a*, *s* levels in $3v_2$ and v_2+v_4, and the transitions in the $3v_2 \leftrightarrow v_2+v_4$, $3v_2 \leftarrow v_2$, $v_2+v_4 \leftarrow v_2$, $3v_2 \leftarrow 2v_2$, $v_2+v_4 \leftarrow 2v_2$, $3v_2 \leftarrow v_4$, and $v_2+v_4 \leftarrow v_4$ hot bands have been predicted, using for the lower levels the term values calculated from the parameters of $v_2 = 1$, 2 and $v_4 = 1$ [27]. The search of these transitions in the spectra was undertaken and resulted greatly facilitated by the precision of their predicted values. Moreover, about one hundred and two hundred perturbation allowed transitions in $v_2+v_4 \leftarrow 2v_2$ and $v_2+v_4 \leftarrow v_2$, respectively, were identified.

Once the assignment work was completed, the vibration-rotation-inversion transitions in the cold and hot bands, 1024 and 4254, respectively, together with 492 inversion and rotation-inversion transitions in $3v_2$ and $v_2 + v_4$ have been analyzed simultaneously. The final data set contains 5770 data, including 395 perturbation allowed transitions. The values of J'_{max} / K'_{max} are comprised between 11/10 to 15/15 depending on the considered band. A summary of the analyzed bands is detailed in Table 1, where the number and characteristics of each sub set are specified. The data set contains a single

Table 1

Transitions analysed in the *a*, *s* inversion levels of $v_2 = 3$ and $v_2 = v_4 = 1$ for $^{15}NH_3$

Band	Type of transitions	Selection rules		No. of lines	J'_{max}	K'_{max}
$3\nu_2 \leftarrow 3\nu_2$	IR inversion	$\Delta J = 0, \Delta k = 0$	$a \leftarrow s$	77	13	13
	FIR + IR rotation-inversion	$\Delta J = \pm 1, \Delta k = 0$	$a \leftarrow s$	138	13	12
$\nu_2 + \nu_4^{\pm 1} \leftarrow \nu_2 + \nu_4^{\pm 1}$	FIR rotation-inversion	$\Delta J = +1, \Delta l = 0, \Delta k = 0$	$a \leftarrow s$, $s \leftarrow a$	116, 161	12, 14	11, 13
$3\nu_2 \leftrightarrow \nu_2 + \nu_4^{\pm 1}$	FIR + IR vibration-rotation-inversion	$\Delta J = 0, \pm 1, \Delta(k-l) = 0$	$s \leftarrow s$, $a \leftarrow a$	246, 220	12, 12	11, 11
$3\nu_2 \leftarrow 2\nu_2$	FIR+IR vibration-rotation-inversion	$\Delta J = 0, \pm 1, \Delta k = 0$	$a \leftarrow s$, $s \leftarrow a$	193, 269	12, 14	12, 14
$\nu_2 + \nu_4^{\pm 1} \leftarrow 2\nu_2$	IR vibration-rotation-inversion	$\Delta J = 0, \pm 1, \Delta(k-l) = 0$	$s \leftarrow s$, $a \leftarrow a$	324, 311	11, 11	11, 11
$\nu_2 + \nu_4^{\pm 1} \leftarrow 2\nu_2$	IR vibration-rotation-inversion	$\Delta J = 0, \pm 1, \Delta(k-l) = \pm 3$	$s \leftarrow a$, $a \leftarrow s$	39, 91	11, 12	10, 10
$3\nu_2 \leftarrow \nu_4^{\pm 1}$	IR vibration-rotation-inversion	$\Delta J = 0, \pm 1, \Delta(k-l) = 0$	$s \leftarrow s$, $a \leftarrow a$	281, 282	11, 12	10, 12
$\nu_2 + \nu_4^{\pm 1} \leftarrow \nu_4^{\pm 1}$	IR vibration-rotation-inversion	$\Delta J = 0, \pm 1, \Delta l = 0, \Delta k = 0$	$a \leftarrow s$, $s \leftarrow a$	385, 374	12, 12	12, 12
$3\nu_2 \leftarrow \nu_2$	IR vibration-rotation-inversion	$\Delta J = 0, \pm 1, \Delta k = 0$	$a \leftarrow s$, $s \leftarrow a$	109, 234	13, 13	13, 13
$\nu_2 + \nu_4^{\pm 1} \leftarrow \nu_2$	IR vibration-rotation-inversion	$\Delta J = 0, \pm 1, \Delta(k-l) = 0$	$s \leftarrow s$, $a \leftarrow a$	352, 355	14, 13	14, 13
$\nu_2 + \nu_4^{\pm 1} \leftarrow \nu_2$	IR vibration-rotation-inversion	$\Delta J = 0, \pm 1, \Delta(k-l) = \pm 3$	$s \leftarrow a$, $a \leftarrow s$	101, 88	12, 12	12, 9
$3\nu_2 \leftarrow GS$	IR vibration-rotation-inversion	$\Delta J = \pm 1, \Delta k = 0$	$a \leftarrow s$, $s \leftarrow a$	194, 218	13, 13	12, 13
$\nu_2 + \nu_4^{\pm 1} \leftarrow GS$	IR vibration-rotation-inversion	$\Delta J = 0, \pm 1, \Delta(k-l) = 0$	$s \leftarrow s$, $a \leftarrow a$	274, 262	14, 15	13, 15
$\nu_2 + \nu_4^{\pm 1} \leftarrow GS$	IR vibration-rotation-inversion	$\Delta J = 0, \pm 1, \Delta(k-l) = \pm 3$	$s \leftarrow a$, $a \leftarrow s$	29, 47	12, 12	8, 11

wavenumber for each assigned transition, choosing the one with the lowest uncertainty in case of alternatives to the present measurements. Our choice is different from that adopted for $^{14}NH_3$ in [20]. The various types of observed transitions are represented in Figure 4 by arrows with different colors in the scheme of the energy states for $^{15}NH_3$, up to 3000 cm^{-1}.

[insert Fig. 4 about here]

3.2 Theoretical model

The theoretical model used for the present analysis is based on the accurate studies on the rotation-inversion Hamiltonian for ammonia [29 and references therein] and on the result of the spectroscopic analysis of $3\nu_2$ and $\nu_2 + \nu_4$ for $^{14}NH_3$ [18,20]. This system was modeled as an interacting dyad, isolated from the network of the nearby vibration excited states [18]. The model was estimated adequate to the analyzed data set, consisting only of cold band transitions, but the larger value of the RMS error for the $3\nu_2$ $a \leftarrow s$ transitions was attributed to the neglect of the interactions with the $\nu_4 = 2$ *s* state, lying just above $\nu_2 = 3$ *a* [18]. Recently, the $3\nu_2$ / $\nu_2 + \nu_4$ dyad of $^{14}NH_3$ has been re-analyzed as an isolated dyad at experimental accuracy thanks to a fairly enlarged data set [20]. The Hamiltonian model adopted in [20] was more extended than that in [18]. It included also the terms of the rotational operators with A_2'' symmetry, classified as "type 3" [20,21], and represented with antisymmetric matrices [29]. The same model was successfully applied in the analysis of $2\nu_2/\nu_4$ in $^{14}NH_3$ [21] and used to analyze the $\nu_2/2\nu_2/\nu_4$ band system in $^{15}NH_3$ [27]. The reproduction of the data set at experimental accuracy was obtained in both isotopologues refining different types and numbers of interaction coefficients.

The relative position of the $\nu_2 = \nu_4 = 1$ and $\nu_2 = 3$ *a*, *s* inversion levels in $^{15}NH_3$ is illustrated in the diagram of Fig. 4. In principle, $\nu_2 = 3$ and $\nu_2 = \nu_4 = 1$ are perturbed by interactions analogous to those active between $\nu_2 = 2$ and $\nu_4 = 1$. Moreover, they could be affected by interactions with states at higher energies, such as $\nu_4 = 2^{0,\pm2}$, *s*, *a* at about 3211 and 3234 cm^{-1} and ($\nu_2 = 2$, $\nu_4 = 1$) *s* at about 3179 cm^{-1}. For $^{15}NH_3$ we decided to adopt the same procedure used in $^{14}NH_3$ and to consider the dyad isolated from the other vibration states, at least as a first approximation to be verified on the basis of the fit results, since the

complexity of the interaction pattern increases very rapidly with increasing energy and density of states. Therefore, the same interaction model used in $v_4 = 1$ and $v_2 = 2$ [27] was applied to $v_2 = v_4 = 1$ and $v_2 = 3$ while the energies of the lower states for the hot band transitions and of the GS were calculated from the very precise spectroscopic parameters in [27], without refining them in the fitting procedure.

For each value of J the program builds four Hamiltonian matrices. Two of them, with $k = 3p$ ($p = 0$, $\pm1, \pm2, \ldots$), are set up for levels of symmetry A' and A'' and contain eigenvalues of A_1', A_2' and A_1'', A_2'' rotational species. We remind that the nuclear spin statistical weight of the A_1' and A_1'' levels is zero. The other two matrices correspond to one of the two (degenerate) blocks of E' and E'' symmetry. The blocks are numerically diagonalized to obtain the energy levels. The diagonal matrix elements, containing the usual contributions up to the 10^{th} power in the angular momentum operators, are given by

$$
\begin{aligned}
{}^{(i)}E_{\mathrm{v}}\left(J,k,l\right)/hc = {}&{}^{(i)}E_{\mathrm{v}}^{0} + {}^{(i)}B_{\mathrm{v}}\left[J\left(J+1\right)-k^2\right] + {}^{(i)}C_{\mathrm{v}}k^2 - 2\,{}^{(i)}\left(C\zeta\right)_{\mathrm{v}}kl - {}^{(i)}D_{\mathrm{v}J}\left[J\left(J+1\right)\right]^2 \\
&- {}^{(i)}D_{\mathrm{v}JK}\left[J\left(J+1\right)\right]k^2 - {}^{(i)}D_{\mathrm{v}K}k^4 + {}^{(i)}\eta_{\mathrm{v}J}\left[J\left(J+1\right)\right]kl + {}^{(i)}\eta_{\mathrm{v}K}k^3l \\
&+ {}^{(i)}H_{\mathrm{v}J}\left[J\left(J+1\right)\right]^3 + {}^{(i)}H_{\mathrm{v}JJK}\left[J\left(J+1\right)\right]^2k^2 + {}^{(i)}H_{\mathrm{v}JKK}\left[J\left(J+1\right)\right]k^4 \\
&+ {}^{(i)}H_{\mathrm{v}K}k^6 + {}^{(i)}L_{\mathrm{v}J}\left[J\left(J+1\right)\right]^4 + {}^{(i)}L_{\mathrm{v}JJJK}\left[J\left(J+1\right)\right]^3k^2 + {}^{(i)}L_{\mathrm{v}JJKK}\left[J\left(J+1\right)\right]^2k^4 \\
&+ {}^{(i)}L_{\mathrm{v}JKKK}\left[J\left(J+1\right)\right]k^6 + {}^{(i)}L_{\mathrm{v}K}k^8 \qquad (1) \\
&+ {}^{(i)}\tau_{\mathrm{v}J}\left[J\left(J+1\right)\right]^2kl + {}^{(i)}\tau_{\mathrm{v}JK}\left[J\left(J+1\right)\right]k^3l + {}^{(i)}\tau_{\mathrm{v}K}k^5l + {}^{(i)}\tau^{*}_{\mathrm{v}K}k^3l^3 \\
&+ {}^{(i)}M_{\mathrm{v}J}\left[J\left(J+1\right)\right]^5 + {}^{(i)}M_{\mathrm{v}JJJJK}\left[J\left(J+1\right)\right]^4k^2 + {}^{(i)}M_{\mathrm{v}JJJKK}\left[J\left(J+1\right)\right]^3k^4 \\
&+ {}^{(i)}M_{\mathrm{v}JJKKK}\left[J\left(J+1\right)\right]^2k^6 + {}^{(i)}M_{\mathrm{v}JKKKK}\left[J\left(J+1\right)\right]k^8 + {}^{(i)}M_{\mathrm{v}K}k^{10}
\end{aligned}
$$

where (i) refers to the parity of the level with respect to the inversion, s or a; $k = \pm K$; $v = v_2 = 3$ or $v_2 = v_4 = 1$; $l = l_4$. All terms containing l vanish for $v_2 = 3$. The off-diagonal matrix elements are reported in the Appendix, where H_{mn} represents a group of terms in the Hamiltonian containing m vibrational operators q_r and/or p_r, and n rotational operators J_α [30]. The subscript of the interaction constants in the Appendix represents the Δk and Δl selection rules for the levels connected by the interaction term in the Hamiltonian. Moreover, a constant without the left superscript (i) corresponds to an $s \leftrightarrow a$ resonance, while an (s) or (a) superscript represents an interaction between levels of the same parity where there is no ambiguity, i.e. ${}^{(s)}q_{22}$, ${}^{(s)}f_{22}^{J}$, ${}^{(s)}f_{22}^{K}$, ${}^{(s)}f_{42}$, ${}^{(s)}f_{42}^{J}$, ${}^{(s)}f_{42}^{K}$, ${}^{(s)}C_{21}^{(2)}$, etc. . For the Coriolis coefficients, ${}^{(i)}C_{11}^{(1)}$, ${}^{(i)}C_{11}^{(2)}$, ${}^{(i)}C_{11}^{(3a)}$ and ${}^{(i)}C_{11}^{(3b)}$, the superscript (i) refers to the parity of the interacting $v_2 = 3$ level. Differently from [20], the (s) and

(*a*) interaction parameters can be refined independently. In the case of the Coriolis type resonances, the coefficients of the H_{31}, H_{32}, H_{33} and H_{34} Hamiltonian terms that connect $v_2 = 3$ and $v_2 = v_4 = 1$ are written with the same symbols used for the coefficients of H_{21}, H_{22}, H_{23} and H_{24}, that connect $v_2 = 1$ and $v_4 = 1$ [27] since in both cases the levels interact according to the same Δk and Δl selection rules. Finally, the β^{222}, β^{24}, and q_{12}^{β} coefficients are related to the "type 3" rotational operators, see Eqs. (27) - (29) in [20]. The computer code and the input data files are available from the authors upon request.

3.3 Analysis

All transitions of the experimental data set were analyzed simultaneously in a least squares treatment refining the parameters of $v_2 = 3$ and $v_2 = v_4 = 1$ in Eq. (1) and in the Appendix. The term values of the lower levels used to calculate the transition wavenumbers were obtained as eigenvalues from the appropriate energy matrices, using the parameters of Table III and IV in [27]. The statistical weight assigned to each experimental datum was proportional to the inverse of its squared estimated uncertainty, quoted 0.0004 cm^{-1} for the FIR wavenumbers and 0.0006 cm^{-1} for the IR ones. The blended transitions were considered affected by uncertainties one order of magnitude larger than those of the isolated lines. Moreover, the weight attributed to each transition was reduced to $1/n$ if n transitions are assigned to the same wavenumber. In total, 535 transitions are blended, representing 9% of the experimental data set.

Several fits were performed refining different sets of parameters. After each iteration, the statistical significance of the obtained parameters was checked as well as their correlation coefficients. All data differing from their corresponding calculated values more than three times their uncertainties were excluded in the last cycle of the fitting procedure. According to this criterion, 134 of 5770 transitions, 2.3%, were discarded. The high quality of the final fit is stated also by the value of the standard deviation of an observation of unit weight, equal to 0.997, confirming the adequacy of the model and of the weight attributed to each datum. The value of the standard deviation of the fit, 0.00057 cm^{-1}, is comparable to the estimated uncertainties of experimental wavenumbers.

4. Discussion

4.1 Fit results

The best set of spectroscopic parameters for the reproduction of the experimental data is listed in Table 2. All parameters are well determined and at least three times larger than their uncertainties. In total, 96 parameters have been refined comprising 4 vibration term values, 28 and 35 diagonal rotational constants of $v_2 = 3$ and $v_2 = v_4 = 1$, respectively, 4 Coriolis interaction coefficients, and 25 interaction coefficients within $v_2 = v_4 = 1$. All parameters of the model listed in Eq. (1) or in the Appendix and not present in Table 2 were nevertheless allowed to vary in the fitting procedure but resulted statistically undetermined or did not improve the fit quality and were constrained to zero.

The percentage differences of the *s* and *a* rotational constants, i.e. $\frac{({}^{(s)}B_v - {}^{(a)}B_v)}{{}^{(s)}B_v} \times 100$, in $v_2 = 3$ and $v_2 = v_4 = 1$ amount to a few percent, very similar to the corresponding values for $^{14}NH_3$ calculated from the results in [20]. For the *D*'s and *H*'s constants the differences are larger, about 13 % and 80 % on average, respectively, for $v_2 = 3$ and 50 %, 150 % on average for $v_2 = v_4 = 1$; these differences are smaller than the corresponding ones for $^{14}NH_3$ [20]. In $v_2 = v_4 = 1$ the *a* and *s* values of the $C\zeta$, η_J and η_K constants are similar, with differences equal to 13 %, 66 % and 121 %, like in $^{14}NH_3$ [20]. Differences larger than 500 % are seen for τ's, indicating that their values are effective.

The comparison of ${}^{(i)}B$ and ${}^{(i)}C$ of $v_2 = 3$ with their corresponding values in $v_2 = 2$ [27] results in the differences –8.7 %, 4.1 %, –5.3 % and 2.0 % for ${}^{(s)}B_v$, ${}^{(s)}C_v$, ${}^{(a)}B_v$ and ${}^{(a)}C_v$, respectively. This suggests that $v_2 = 3$ *a* is less perturbed than the *s* state, as expected from the energy differences among the states depicted in the scheme of Fig. 4.

Table 2

Spectroscopic parameters (in cm^{-1}) of the *a*, *s* levels for $v_2 = 3$ and $v_2 = v_4 = 1$ of $^{15}NH_3$ [a]

Parameter	$v_2 = 3$ *s*	$v_2 = 3$ *a*	$v_2 = v_4^{\pm 1} = 1$ *s*	$v_2 = v_4^{\pm 1} = 1$ *a*
E^0	2369.31094965(6970)	2876.12237870(8867)	2533.37170600(5393)	2577.60209315(5934)
B	9.491814403(5661)	9.183567670(8274)	10.295679275(3243)	10.085203170(3658)
C	6.188526799(6840)	6.293078978(9228)	6.019095329(5974)	6.107631892(6166)
$D_J \times 10^3$	−0.3069898(1487)	−0.2926392(2374)	1.35950983(6712)	0.88217899(7597)
$D_{JK} \times 10^3$	1.3833895(3441)	1.2849612(4904)	−2.9695282(3493)	−1.6206689(4034)
$D_K \times 10^3$	−0.9980653(2411)	−0.8691379(3307)	1.8613189(3772)	0.9249684(3069)
$H_J \times 10^6$	−0.792684(1696)	−1.108884(2416)	0.5728193(7387)	0.2355758(3266)
$H_{JJK} \times 10^6$	2.405837(6419)	4.068545(7224)	−2.833416(3074)	−0.321250(1808)
$H_{JKK} \times 10^6$	−2.316988(8361)	−4.878648(8631)	4.404873(4588)	0.135143(3549)
$H_K \times 10^6$	0.728903(3778)	1.982941(4009)	−2.059068(3078)	0.012096(2668)
$L_J \times 10^9$	1.847675(4465)	2.195386(8199)	0.0 [b]	0.0 [b]
$L_{JJJK} \times 10^9$	−9.82608(2613)	−11.10118(3221)	0.0 [b]	0.0 [b]
$L_{JJKK} \times 10^9$	19.28282(5670)	20.20021(5879)	1.93605(1832)	−0.82866(1322)
$L_{JKKK} \times 10^9$	−16.47802(5300)	−15.96523(5138)	− 3.50055(3458)	0.82410(1278)
$L_K \times 10^9$	4.94983(1879)	4.40440(1937)	1.48841(1970)	0.0 [b]
$C\zeta$			−1.268202351(9330)	−1.448315310(9295)
$\eta_J \times 10^3$			−1.917047(1165)	−3.8207378(8730)
$\eta_K \times 10^3$			0.861346(1017)	3.4965442(7883)
$\tau_J \times 10^6$			−11.59473(2226)	24.81180(4468)
$\tau_{JK} \times 10^6$			38.60717(6335)	−37.9875(1205)
$\tau_K \times 10^6$			−27.44445(5662)	13.10092(8019)

Interaction parameters

$v_2 = 3$ / $v_2 = v_4^{\pm 1} = 1$

$^{(s)}C_{21}^2$	0.01925939(7109)	$^{(a)}C_{21}^2$	0.02134628(4015)
$^{(s)}C_{21}^{4a} \times 10^3$	0.1830941(7060)	$^{(s)}C_{21}^{4b} \times 10^3$	− 0.2634022(6644)

$v_2 = v_4^{\pm 1} = 1$

$^{(s)}q_{22}$	0.062762212(1832)	$f_{12}^{KK}\times10^{6}$	0.393104(1863)
$^{(a)}q_{22}$	0.070681922(1968)	$^{(s)}f_{42}\times10^{3}$	−0.02778664(6008)
$^{(s)}f_{22}^{J}\times10^{3}$	−0.03385611(3399)	$^{(a)}f_{42}\times10^{3}$	−0.00129499(6073)
$^{(a)}f_{22}^{J}\times10^{3}$	−0.04982473(3549)	$^{(s)}f_{42}^{J}\times10^{6}$	0.1557594(7610)
$^{(s)}f_{22}^{K}\times10^{3}$	−0.1985332(3571)	$^{(a)}f_{42}^{J}\times10^{6}$	−0.040337(1014)
$^{(a)}f_{22}^{K}\times10^{3}$	0.1599375(4002)	$^{(s)}f_{42}^{K}\times10^{6}$	1.899049(2706)
$^{(s)}f_{22}^{JJ}\times10^{6}$	−0.0987167(1593)	$^{(a)}f_{42}^{K}\times10^{6}$	2.771315(3363)
$^{(a)}f_{22}^{JJ}\times10^{6}$	0.0676039(1832)	$^{(s)}f_{42}^{JJ}\times10^{9}$	0.830738(3123)
$^{(s)}f_{22}^{JK}\times10^{6}$	−0.203083(1249)	$^{(a)}f_{42}^{JJ}\times10^{9}$	−1.557916(4591)
q_{12}	−0.057213107(3716)	$\alpha^{24}\times10^{3}$	0.2295359(1435)
$f_{12}^{J}\times10^{3}$	0.07430664(3012)	$\alpha_{J}^{24}\times10^{6}$	0.334668(1066)
$f_{12}^{K}\times10^{3}$	0.0408015(3086)	$\alpha_{K}^{24}\times10^{6}$	−2.296617(7480)
$f_{12}^{JK}\times10^{6}$	−0.256139(2375)		
Total number of assigned/fitted transitions	5770/5636		
Standard deviation of an observation of unit weight	0.997		

[a] The uncertainties as 1σ given in parentheses refer to the last significant digits and are reported with 4 digits to avoid round off errors in the calculation of the transition wavenumbers.
[b] Constrained, see text.

For the $^{(i)}D$'s centrifugal distortion constants we noticed that the values of $^{(i)}D_J$ and $^{(i)}D_K$ in $v_2 = 3$ have the same order of magnitude than in $v_2 = 2$ while for $^{(i)}D_{JK}$ they are one order of magnitude larger. A peculiarity concerns the signs of D's in $v_2 = 3$ which are opposite with respect to those in $v_2 = 2$; the same is observed in $^{14}NH_3$ [18,20].

The number of interaction parameters whose role was significant for the fit quality is smaller than in case of $2\nu_2 /\nu_4$ [27]. The values of the $^{(i)}C_{21}^2$ Coriolis coefficients in the dyad $3\nu_2/\nu_2+\nu_4$ are similar to the ones in $2\nu_2/\nu_4$; $^{(i)}q_{22}$ and $^{(s)}f_{42}$ are about one order of magnitude larger than those in $v_4 = 1$, while $^{(a)}f_{42}$ is one third that in $v_4 = 1$. q_{12} is smaller with opposite sign and α^{24} is about two times α^4 [27].

Few significant correlations, lower than 100%, are present among the parameters and concern only the centrifugal distortion constants L's and the higher order dependences of $^{(a)}\eta$, $^{(a)}q_{22}$ and $^{(a)}f_{42}$. The $^{(a)}f_{22}^K$ coefficient is 99% correlated to $^{(a)}\tau_J$, $^{(a)}L_{v2=3,J}$ is 99 % correlated to $^{(a)}H_{v2=3,J}$, while correlations equal to 98% are observed between: $^{(a)}L_{v2=v4=1,JKKK}$ and $^{(a)}L_{v2=v4=1,JJKK}$, $^{(a)}\tau_K$ and $^{(a)}\tau_{JK}$, and $^{(a)}f_{42}^{JJ}$, $^{(a)}f_{42}^{J}$.

The spectroscopic parameters in Table 2 reproduce adequately the experimental data set as can be inferred from the RMS errors listed in Table 3. They have been calculated considering the unblended transitions assigned to the studied bands and their values are in good agreement with the uncertainties attributed to the data in the least squares procedure.

Table 3
The RMS values of the fit for the sub sets of transitions to $v_2 = 3$ and $v_2 = v_4 = 1$ of $^{15}NH_3$

Band		assigned / fitted transitions	J'_{max}	K'_{max}	RMS / 10^{-3} cm^{-1}
$3\nu_2$	$a \leftarrow s$	194 / 192	13	12	0.60
	$s \leftarrow a$	218 / 216	13	13	0.64
$3\nu_2 \leftarrow 3\nu_2$	$a \leftarrow s$	215 / 215	13	13	0.39
$3\nu_2 \leftarrow 2\nu_2$	$a \leftarrow s$	193 / 193	12	12	0.56
	$s \leftarrow a$	269 / 269	14	14	0.44
$3\nu_2 \leftarrow \nu_2$	$a \leftarrow s$	109 / 109	13	13	0.57
	$s \leftarrow a$	234 / 234	13	13	0.58
$3\nu_2 \leftarrow \nu_2 + \nu_4^{-1}$	$a \leftarrow a$	115 /115	11	11	0.40
$3\nu_2 \leftarrow \nu_2 + \nu_4^{+1}$	$a \leftarrow a$	105 /105	12	10	0.45

$3\nu_2 \leftarrow \nu_4^{-1}$	$s \leftarrow s$	146 / 146	10	10	0.65
	$a \leftarrow a$	133 / 133	12	12	0.58
$3\nu_2 \leftarrow \nu_4^{+1}$	$s \leftarrow s$	135 / 135	11	9	0.60
	$a \leftarrow a$	149 / 149	12	10	0.62
$\nu_2+\nu_4^{-1}$	$s \leftarrow s$, $s \leftarrow a$	160 / 149	12	10	0.76
	$a \leftarrow a$, $a \leftarrow s$	148 / 135	11	11	0.77
$\nu_2+\nu_4^{+1}$	$s \leftarrow s$, $s \leftarrow a$	143 / 139	14	13	0.65
	$a \leftarrow a$, $a \leftarrow s$	161 / 149	15	15	0.82
$\nu_2+\nu_4^{-1} \leftarrow 3\nu_2$	$s \leftarrow s$	142 / 137	12	10	0.43
$\nu_2+\nu_4^{+1} \leftarrow 3\nu_2$	$s \leftarrow s$	104 / 101	11	11	0.43
$\nu_2+\nu_4^{-1} \leftarrow 2\nu_2$	$s \leftarrow s$, $s \leftarrow a$	200 / 193	12	11	0.62
	$a \leftarrow a$, $a \leftarrow s$	218 / 212	12	11	0.64
$\nu_2+\nu_4^{+1} \leftarrow 2\nu_2$	$s \leftarrow s$, $s \leftarrow a$	163 / 157	11	11	0.53
	$a \leftarrow a$, $a \leftarrow s$	184 / 180	12	11	0.57
$\nu_2+\nu_4^{-1} \leftarrow \nu_2$	$s \leftarrow s$, $s \leftarrow a$	267 / 258	12	12	0.62
	$a \leftarrow a$, $a \leftarrow s$	241 / 234	12	11	0.62
$\nu_2+\nu_4^{+1} \leftarrow \nu_2$	$s \leftarrow s$, $s \leftarrow a$	186 / 179	14	14	0.56
	$a \leftarrow a$, $a \leftarrow s$	202 / 198	13	13	0.60
$\nu_2+\nu_4^{-1} \leftarrow \nu_4^{-1}$	$s \leftarrow a$	214 /205	12	12	0.63
	$a \leftarrow s$	219 / 213	12	12	0.69
$\nu_2+\nu_4^{+1} \leftarrow \nu_4^{+1}$	$s \leftarrow a$	160 / 154	12	11	0.51
	$a \leftarrow s$	166 / 160	12	11	0.57
$\nu_2+\nu_4^{+1} \leftarrow \nu_2+\nu_4^{+1}$	$s \leftarrow a$	77 / 75	14	13	0.39
	$a \leftarrow s$	49 / 48	12	10	0.45
$\nu_2+\nu_4^{-1} \leftarrow \nu_2+\nu_4^{-1}$	$s \leftarrow a$	84 / 83	14	13	0.40
	$a \leftarrow s$	67 / 66	12	11	0.42

The transition wavenumbers, assignments and residuals calculated using the parameters in Table 2 for the upper states and in Tables III and IV of [27] for the lower states, are listed in order of increasing energy in Table S1 of the Supplementary materials. In Table S2 the data set is divided into three portions listed for increasing J', grouping the transitions according to the upper vibration state. The transitions discarded in the last cycle of refinement are identified by ***. We remind that the assignments in Tables S1 and S2 are, in a few cases, only formal, since k–l_4 and not k is a good quantum number for the system of interacting levels. The principle of the largest contribution of the unperturbed wavefunctions to the perturbed levels has been adopted to assign a transition to a particular upper level.

It can be noticed that about 90% of the 134 rejected transitions in Table S2 are not randomly distributed. They reach the following J' / K' rotational levels: 4/2, 5/2, 7/2 *s* and 6/2, 8/7 *a*, in $v_2 = v_4 = 1$, $l_4 =$

−1, while in $v_2 = v_4 = 1$ $l_4 = +1$ reach the 7/2, 9/5 *s* and 7/4 *a* levels. The differences between experimental and calculated wavenumbers of those transitions amount to about 3.6 x 10^{-3} cm^{-1} on average, while amount to 2.7 x 10^{-2} cm^{-1} for transitions to 7/2 *s* and 6/2 *a*, $l_4 = -1$ levels. The listed levels are not connected by perturbations in the adopted model and the term values of possible partners of interactions are nicely reproduced. All attempts to better reproduce the rejected transitions, whose assignments we confidently trust, failed.

The comparison of the $3v_2/v_2+v_4$ spectroscopic parameters for $^{15}NH_3$ and $^{14}NH_3$ [18, 20] can be accomplished considering also the differences among the experimental data bases. Only transitions of the $3v_2$ and v_2+v_4 cold bands of $^{14}NH_3$ were analyzed in [18]. An extended data set, comprising literature [18, 22] and newly assigned hot band transitions and inversion-rotation transitions was analyzed in [20]. The distribution among the different bands of the experimental unique transitions, about 2400 of 3422 from the line list [20], is detailed in Table 4. The corresponding information on $^{15}NH_3$ are also collected in the table for comparison. In the overall, the number of experimental data of $^{15}NH_3$ is about two times larger than that of $^{14}NH_3$. The main differences are the number of hot band transitions and of the perturbation allowed ones, larger in $^{15}NH_3$, while the reverse is true on the whole for the assignments to cold bands. The values of J'_{max} / K'_{max} are similar in various bands for the two isotopologues but the amount of information from experiment is more complete in $^{15}NH_3$.

Table 4
Comparison of the data sets constituted by unique transitions for $3v_2/v_2+v_4$ of $^{14}NH_3$[a] and $^{15}NH_3$

		$^{14}NH_3$		$^{15}NH_3$	
Band		assigned/fitted transitions	J'_{max} / K'_{max}	assigned/fitted transitions	J'_{max} / K'_{max}
$3v_2$	$a \leftarrow s$	225 [b]/216	12/12	194/192	13/12
	$s \leftarrow a$	219 [b] /218	12/12	218/216	13/13
$3v_2 \leftarrow 3v_2$	$a \leftarrow s$	224 [a] /224	13/12	215/215	13/13
$3v_2 \leftarrow 2v_2$	$a \leftarrow s$	191 [a] /191	13/12	193/193	12/12
	$s \leftarrow a$	260 [a] /260	15/13	269/269	14/14
	$s \leftarrow s$	1 [a] /1	14/13	-	-
$3v_2 \leftarrow v_2$	$a \leftarrow s$	65 [c] /50	10/10	109/109	13/13
	$s \leftarrow a$	60 [a,c] /48	14/10	234/234	13/13

	$s \leftarrow s$	1 [c] /1	10/8	-	-
$3\nu_2 \leftarrow \nu_2 + \nu_4^{-1}$	$a \leftarrow a$	-	-	115/115	11/11
$3\nu_2 \leftarrow \nu_2 + \nu_4^{+1}$	$a \leftarrow a$	-	-	105/105	12/10
$3\nu_2 \leftarrow \nu_4^{-1}$	$s \leftarrow s$	4 [a] /4	8/7	146/146	10/10
	$s \leftarrow a$	1 [a] /1	13/9	-	-
	$a \leftarrow a$	-	-	133/133	12/12
$3\nu_2 \leftarrow \nu_4^{+1}$	$s \leftarrow s$	-	-	135/135	11/9
	$a \leftarrow a$	12 [a] /12	13/12	149/149	12/10
$\nu_2 + \nu_4^{-1}$	$s \leftarrow s$	174 [b] /159	12/11	141/130	11/10
	$s \leftarrow a$	69 [b] /67	11/10	19/19	12/5
	$a \leftarrow a$	178 [b] /167	12/12	118/105	10/10
	$a \leftarrow s$	62 [b] /58	11/11	30/30	11/11
$\nu_2 + \nu_4^{+1}$	$s \leftarrow s$	172 [b] /165	13/13	133/129	14/13
	$s \leftarrow a$	51 [b] /46	12/8	10/10	12/8
	$a \leftarrow a$	171 [b] /156	13/13	144/132	15/15
	$a \leftarrow s$	39 [b] /34	12/7	17/17	12/8
$\nu_2 + \nu_4^{-1} \leftarrow 3\nu_2$	$s \leftarrow s$	1 [a] /1	5/0	142/137	12/10
$\nu_2 + \nu_4^{+1} \leftarrow 3\nu_2$	$s \leftarrow s$	-	-	104/101	11/11
$\nu_2 + \nu_4^{-1} \leftarrow 2\nu_2$	$s \leftarrow s$	6 [a] /6	9/5	169/162	11/11
	$a \leftarrow a$	2 [a] /2	3/2	164/159	11/11
	$a \leftarrow s$	1 [a] /1	8/5	54/53	12/11
	$s \leftarrow a$	-	-	31/31	12/10
$\nu_2 + \nu_4^{+1} \leftarrow 2\nu_2$	$s \leftarrow s$	23 [a] /23	14/13	155/149	11/11
	$a \leftarrow a$	4 [a] /4	11/10	147/144	11/11
	$a \leftarrow s$	-	-	37/36	12/10
	$s \leftarrow a$	-	-	8/8	11/7
$\nu_2 + \nu_4^{-1} \leftarrow \nu_2$	$s \leftarrow s$	-	-	191/182	12/12
	$a \leftarrow a$	-	-	188/183	12/11
	$a \leftarrow s$	-	-	53/51	12/9
	$s \leftarrow a$	-	-	76/76	12/12
$\nu_2 + \nu_4^{+1} \leftarrow \nu_2$	$s \leftarrow s$	-	-	161/155	14/14
	$a \leftarrow a$	-	-	167/164	13/13
	$a \leftarrow s$	-	-	35/34	12/8
	$s \leftarrow a$	-	-	25/24	11/9
$\nu_2 + \nu_4^{-1} \leftarrow \nu_4^{+1}$	$s \leftarrow a$	2 [a] /2	9/5	-	-
$\nu_2 + \nu_4^{-1} \leftarrow \nu_4^{-1}$	$s \leftarrow a$	6 [a] /6	8/2	214/205	12/12
	$a \leftarrow s$	-	-	219/213	12/12
$\nu_2 + \nu_4^{+1} \leftarrow \nu_4^{+1}$	$s \leftarrow a$	22 [a] /22	12/10	160/154	12/11
	$a \leftarrow s$	-	-	166/160	12/11
$\nu_2 + \nu_4^{+1} \leftarrow \nu_2 + \nu_4^{+1}$	$s \leftarrow a$	55 [a] /54	15/14	77/75	14/13
	$s \leftarrow s$	4 [a] /4	10/4	-	-
	$a \leftarrow s$	38 [a] / 38	13/11	49/48	12/10
	$s \leftarrow a$	62 [a] /58	14/11	84/83	14/13

	$s \leftarrow s$	5 [a] /5	10/0	-	-
	$a \leftarrow s$	47 [a] / 47	12/9	67/66	12/11
$\nu_2+\nu_4^{-1} \leftarrow \nu_2+\nu_4^{+1}$	$s \leftarrow s$	16 [a] /14	13/8	-	-
	$s \leftarrow a$	1 [a] /1	12/3	-	-
$\nu_2+\nu_4^{+1} \leftarrow \nu_2+\nu_4^{-1}$	$s \leftarrow s$	40 [a] /39	13/9	-	-

[a] From Ref. [20];
[b] From Ref. [18];
[c] From Ref. [22].

The model Hamiltonian used in our analysis is equal to that in [20] and both are more extended than that applied in [18]. Kleiner et al. determined 48 spectroscopic parameters, 36 vibration-rotation-inversion and the α^{24}, α^{222}, ${}^{(i)}q_{22}$, ${}^{(i)}f_{22}^{J}$, ${}^{(i)}f_{22}^{K}$, q_{12}, f_{12}^{J}, f_{12}^{K}, ${}^{(i)}f_{42}$, ${}^{(i)}C_{21}^{2}$ interaction constants [18]. The extension of the data base and the purpose of reproducing it at experimental accuracy increased to 147 the number of parameters determined by Pearson et al. [20], 109 diagonal constants and 38 interaction coefficients. Of these, the leading coefficients, according to our notation, are ${}^{(i)}\eta_3^{222}$, ${}^{(i)}\eta_3^{24}$, α^{222}, α^{24}, ${}^{(i)}q_{22}$, q_{12}, ${}^{(i)}f_{42}$, the Coriolis ${}^{(i)}C_{11}^{(1)}$, ${}^{(i)}C_{11}^{(2)}$, ${}^{(i)}C_{21}^{2}$, and the q_{12}^{β}, β^{24} parameters from a "type 3" rotational operator with A_2'' symmetry [20, 21, 27, 29]. The comparison of the values of the same diagonal and interaction coefficients reported in [20] and [18] results in a fairly good agreement [20].

In the present work we determined 96 parameters, 67 diagonal and 29 interaction coefficients. This set is similar to that in [18] for the type of the Coriolis-coupling and $\Delta l = 0, \Delta k = \pm 3$ coefficients, ${}^{(i)}C_{21}^{2}$ and α^{24}, while to that in [20] for the higher order centrifugal distortion constants in Eq. (1) and the essential resonances in $v_2 = v_4 = 1$. The ${}^{(i)}q_{22}$, q_{12}, and ${}^{(i)}f_{42}$ coefficients with their higher order dependences play a very important role to adequately reproduce the term values of the *a*, *s* inversion levels in $v_2 = v_4 = 1$ for both $^{15}NH_3$ and $^{14}NH_3$.

A comparison of the values for some parameters in Table 2 with those of $^{14}NH_3$ [20] is presented in Table 5. ${}^{(i)}B$, ${}^{(i)}C$ and ${}^{(i)}C\zeta$ are very similar and close values are observed also for the ${}^{(i)}D$'s. Large differences are observed for the η's constants since more high order dependences are determined in [20]. The α^{24} values are almost equal while q_{12} of $^{15}NH_3$ is about one third that of $^{14}NH_3$. Their signs are opposite in the two isotopologues but this has no consequences since they are relative. In fact, identical energies for the ro-

vibration levels and identical intensities for the transitions are calculated from the four equivalent sets obtained by multiplying the parameters ${}^{(i)}C_{11}^{1}$, ${}^{(i)}C_{11}^{2}$, ${}^{(i)}C_{11}^{3a}$, ${}^{(i)}C_{11}^{3b}$ by the coefficient $\gamma = \pm 1$, α^{24}, α_J^{24}, α_K^{24}, q_{12}, f_{12}^{J}, f_{12}^{K} by $\gamma' = \pm 1$, and ${}^{(i)}C_{21}^{2}$, ${}^{(i)}C_{21}^{3}$, ${}^{(i)}C_{21}^{4a}$, ${}^{(i)}C_{21}^{4b}$ by $\gamma\gamma'$. Both ${}^{(s)}q_{22}$ and ${}^{(a)}q_{22}$ have half values and opposite signs with respect to $^{14}NH_3$. The sign difference could be due to the determination in [20] of the Coriolis parameter ${}^{(s)}C_{11}^{1}$ which is usually strongly correlated to ${}^{(i)}q_{22}$. In fact, signs identical to ours were obtained for ${}^{(i)}q_{22}$ in [18] where ${}^{(i)}C_{11}^{1}$ was not refined. The values of ${}^{(i)}C_{21}^{2}$ are comparable in the two isotopologues, the major differences being that we refined independently ${}^{(s)}C_{21}^{2}$ and ${}^{(a)}C_{21}^{2}$ while a single value is reported in [20].

Table 5
Comparison of some molecular parameters (in cm^{-1}) of the *a*, *s* levels for $v_2 = 3$ and $v_2 = v_4 = 1$ for $^{15}NH_3$ and $^{14}NH_3$ [a]

Parameter	$^{14}NH_3$		$^{15}NH_3$	
	$v_2 = 3$ *s*	$v_2 = 3$ *a*	$v_2 = 3$ *s*	$v_2 = 3$ *a*
B	9.522127(8)	9.181836(9)	9.491814(6)	9.183567(8)
C	6.19590(5)	6.29322(3)	6.188527(7)	6.293079(9)
$D_J \times 10^3$	−0.2305(5)	−0.2728(4)	−0.3070(1)	−0.2926(2)
$D_{JK} \times 10^3$	0.762(7)	1.604(5)	1.3834(3)	1.2850(5)
$D_K \times 10^3$	−0.479(7)	−1.196(4)	−0.9981(2)	−0.8691(3)
$\alpha^{222} \times 10^3$	−0.562(8)		0.0	
	$v_2 = v_4 = 1$ *s*	$v_2 = v_4 = 1$ *a*	$v_2 = v_4 = 1$ *s*	$v_2 = v_4 = 1$ *a*
B	10.32452(2)	10.09122(3)	10.295679(3)	10.085203(4)
C	6.01564(4)	6.11042(7)	6.019095(6)	6.107632(6)
$D_J \times 10^3$	1.3343(5)	0.8115(7)	1.35951(7)	0.88218(8)
$D_{JK} \times 10^3$	−3.176(5)	−1.102(8)	−2.9695(3)	−1.6207(4)
$D_K \times 10^3$	2.103(6)	0.456(7)	1.8613(4)	0.9250(3)
$C\zeta$	−1.30723(1)	−1.47932(2)	−1.268202(9)	−1.448315(9)
$\eta_J \times 10^3$	−3.34(2)	−0.81(3)	−1.917(1)	−3.8207(9)

$\eta_K \times 10^3$	2.48(2)	0.13(3)	0.861(1)	3.4965(8)
$\alpha^{24} \times 10^3$	–0.2575(7)		0.2295(1)	
q_{12}	0.2198(3)		–0.057213(4)	
${}^{(s)}q_{22}$	–0.13155(2)		0.062762(2)	
${}^{(a)}q_{22}$	–0.13155(2)		0.070682(2)	
${}^{(s)}f_{42} \times 10^3$	0.01846(4)		–0.02779(6)	
${}^{(a)}f_{42} \times 10^3$	0.01846(4)		–0.00129(6)	
${}^{(s)}C_{21}^2$	0.03276(9)		0.01926(7)	
${}^{(a)}C_{21}^2$	0.03276(9)		0.02135(4)	

[a] Ref [20]

4.2 Comparison between observed and theoretically calculated transitions

All the assigned transitions of the cold and hot bands and the rotation-inversion transitions in $v_2 = 3$ and $v_2 = v_4 = 1$ are compared with the *ab initio* line list, from the best compilation at room temperature available up to now for $^{15}NH_3$ by Yurchenko [26], that includes positions and intensities up to $J' = 18$. The comparisons are reported in Tables S3 to S14 supplied as Supplementary material. In some cases more than one theoretically calculated wavenumber was attributed to a given transition due to the criterion adopted for labeling the term values which is based on the largest contribution of a particular basis level among those present in the eigenvector [26]. In those cases, we discriminated between the various alternatives in [26] by selecting the calculated value closest to the observed one. Another critical problem was faced in $v_2 = v_4 = 1$ since only the absolute value of the vibration quantum number l_4 is reported in the *ab initio* line list. The sign of l_4 was added in Tables S7 - S14 according to the experimental results. For some of the assigned transitions no prediction was found in [26]. Owing to the uncertainty in the prediction of both the wavenumber and the rotation-inversion identity of the levels involved in the transitions, we could not exploit the theoretical predictions to extend the assignment to larger J values.

The agreement between observed and calculated wavenumbers is reasonable, with RMS error equal to 0.295 cm^{-1} for 413 data of $3v_2$, and 1.687 cm^{-1} for 609 data of $v_2 + v_4$. The values of the RMS errors for the hot bands, in cm^{-1}, are: 0.182 for 343 data of $3v_2 \leftarrow v_2$, 0.876 for 495 data of $3v_2 \leftarrow 2v_2$, 2.054 for 220

data of $3\nu_2 \leftarrow \nu_2 + \nu_4$, 1.054 for 548 data of $3\nu_2 \leftarrow \nu_4$, 9.298 for 895 data of $\nu_2 + \nu_4 \leftarrow \nu_2$, 2.747 for 758 data of $\nu_2 + \nu_4 \leftarrow \nu_4$, 14.564 for 747 data of $\nu_2 + \nu_4 \leftarrow 2\nu_2$, and 2.497 for 246 data of $\nu_2 + \nu_4 \leftarrow 3\nu_2$. The values of the RMS errors for the inversion-rotation transitions in $\nu_2 = 3$ and $\nu_2 = \nu_4 = 1$ are 0.095 and 1.804 cm^{-1}, for 202 and 277 data, respectively.

The large RMS values are due to a few transitions whose observed minus calculated differences are very large. Neglecting these values in the RMS calculation, the agreement improves considerably to 0.215 cm^{-1} (604 data of $\nu_2 + \nu_4$), 0.161 cm^{-1} (455 data of $3\nu_2 \leftarrow 2\nu_2$), 0.106 cm^{-1} (216 data of $3\nu_2 \leftarrow \nu_2 + \nu_4$), 0.234 cm^{-1} (541 data of $3\nu_2 \leftarrow \nu_4$), 0.129 cm^{-1} (780 data of $\nu_2 + \nu_4 \leftarrow \nu_2$), 0.238 cm^{-1} (719 data of $\nu_2 + \nu_4 \leftarrow \nu_4$), 0.356 cm^{-1} (658 data of $\nu_2 + \nu_4 \leftarrow 2\nu_2$), 0.089 cm^{-1} (242 data of $\nu_2 + \nu_4 \leftarrow 3\nu_2$), and 0.211 cm^{-1} (263 data in $\nu_2 = \nu_4 = 1$).

5. Conclusions

The study of the vibration bending states at low energy for $^{15}NH_3$ [27] is extended in this work to the *a*, *s* inversion levels of $\nu_2 = 3$ and $\nu_2 = \nu_4 = 1$ states. High resolution IR spectra from 60 to 2000 cm^{-1} have been recorded using the high sensitivity instrumental capabilities at the Canadian Light Source, while the $3\nu_2$ and $\nu_2 + \nu_4$ cold bands have been observed in the new FTIR spectra measured in Bologna. Thanks to a careful work of assignments a nearly complete experimental data base with J' and K' up to 15 has been obtained. It is constituted by the transitions of $3\nu_2$ and $\nu_2 + \nu_4$, of all the hot bands with $\nu_2 = 1$, 2 or $\nu_4 = 1$ as lower states and $3\nu_2 \leftrightarrow \nu_2 + \nu_4$, and of the rotation-inversion transitions in $\nu_2 = 3$ and $\nu_2 = \nu_4 = 1$. Altogether, 5636 non-zero weighted data, including about 7% of perturbation allowed ones, have been fitted to 96 highly precise spectroscopic parameters, 67 diagonal and 29 off-diagonal coefficients using the model Hamiltonian applied in [27] for $^{15}NH_3$ and in [20] for $^{14}NH_3$. The reproduction of wavenumbers at experimental accuracy is attained using a small number of parameters, all statistically well determined, and surveying the presence of severe internal correlations. Lists of assigned transitions have been supplied as Supplementary material. The comparison of all the transitions with their corresponding theoretical predictions [26] revealed satisfactory agreement in some cases, but evidenced also pitfalls concerning the

labeling of the levels of $v_2 = v_4 = 1$. Tables of all these comparisons are supplied as Supplementary material. The present results noticeably improve the wavenumber line list for $^{15}NH_3$ in the HITRAN data base [28]. It is our hope that the obtained new data will further stimulate the search for detection of this molecule in space.

Appendix

Off–diagonal matrix elements of the vibration–rotation–inversion Hamiltonian [a]

The basis functions are $\begin{matrix} {}^{s}_{a}|\, \mathrm{v}_2 \mathrm{v}_4^{l_4}, J, k\rangle = {}^{s}_{a}|\, 30^0, J, k\rangle = {}^{s}_{a}|\, 3\nu_2, J, k\rangle; \\ {}^{s}_{a}|\, \mathrm{v}_2 \mathrm{v}_4^{l_4}, J, k\rangle = {}^{s}_{a}|\, 11^{\pm 1}, J, k\rangle = {}^{s}_{a}|\, \nu_2 + \nu_4^{\pm 1}, J, k\rangle \end{matrix}$

Coriolis type resonances

$$ {}^{s}_{a}\left\langle 3\nu_2, J, k \left| (H_{31} + H_{33})/hc \right| \nu_2 + \nu_4^{\pm 1}, J, k \pm 1 \right\rangle^{a}_{s} = \pm\sqrt{2}\left\{ {}^{(i)}C_{11}^{1} + {}^{(i)}C_{11}^{3a} J(J+1) + {}^{(i)}C_{11}^{3b}\left[k^2 + (k \pm 1)^2 \right] \right\} F_{\pm 1} $$

$$ {}^{s}_{a}\left\langle 3\nu_2, J, k \left| (H_{32} + H_{34})/hc \right| \nu_2 + \nu_4^{\pm 1}, J, k \pm 1 \right\rangle^{a}_{s} = \sqrt{2}\left\{ \left[{}^{(i)}C_{11}^{2} + {}^{(i)}C_{11}^{4a} J(J+1) \right](2k \pm 1) + {}^{(i)}C_{11}^{4b}\left[k^3 + (k \pm 1)^3 \right] \right\} F_{\pm 1} $$

$$ {}^{s}_{a}\left\langle 3\nu_2, J, k \left| (H_{32} + H_{34})/hc \right| \nu_2 + \nu_4^{\mp 1}, J, k \pm 2 \right\rangle^{s}_{a} = \sqrt{2}\left\{ {}^{(i)}C_{21}^{2} + {}^{(i)}C_{21}^{4a} J(J+1) + {}^{(i)}C_{21}^{4b}\left[k^2 + (k \pm 2)^2 \right] \right\} F_{\pm 2} $$

$$ {}^{s}_{a}\left\langle 3\nu_2, J, k \left| H_{33}/hc \right| \nu_2 + \nu_4^{\mp 1}, J, k \pm 2 \right\rangle^{s}_{a} = \pm\sqrt{2}\, {}^{(i)}C_{21}^{3}(2k \pm 2) F_{\pm 2} $$

$$ {}^{s}_{a}\left\langle 3\nu_2, J, k \left| H_{34}/hc \right| \nu_2 + \nu_4^{\mp 1}, J, k \mp 4 \right\rangle^{s}_{a} = \pm\left\{ {}^{(i)}C_{41}^{4} + {}^{(i)}C_{41}^{4a} J(J+1) \right\} F_{\pm 4} $$

$\Delta l = 0,\ \Delta k = \pm 3$ and $\Delta l = 0,\ \Delta k = \pm 6$ type resonances

$$ {}^{s}_{a}\left\langle 3\nu_2, J, k \left| (H_{04} + H_{24} + H_{26})/hc \right| 3\nu_2, J, k \pm 3 \right\rangle^{a}_{s} = \left\{ \begin{matrix} \left[\alpha^{222} + \alpha_J^{222} J(J+1) + \alpha_{JJ}^{222} J^2 (J+1)^2 \right](2k \pm 3) + \\ \left[\alpha_K^{222} + \alpha_{JK}^{222} J(J+1) \right]\left[k^3 + (k \pm 3)^3 \right] + \alpha_{KK}^{222}\left[k^5 + (k \pm 3)^5 \right] \end{matrix} \right\} F_{\pm 3} $$

$$ {}^{s}_{a}\left\langle \nu_2 + \nu_4^{\pm 1}, J, k \left| (H_{04} + H_{24} + H_{26})/hc \right| \nu_2 + \nu_4^{\pm 1}, J, k \pm 3 \right\rangle^{a}_{s} = \left\{ \begin{matrix} \left[\alpha^{24} + \alpha_J^{24} J(J+1) + \alpha_{JJ}^{24} J^2 (J+1)^2 \right](2k \pm 3) + \\ \left[\alpha_K^{24} + \alpha_{JK}^{24} J(J+1) \right]\left[k^3 + (k \pm 3)^3 \right] + \alpha_{KK}^{24}\left[k^5 + (k \pm 3)^5 \right] \end{matrix} \right\} F_{\pm 3} $$

$$ {}^{s}_{a}\left\langle \nu_2 + \nu_4^{\pm 1}, J, k \left| (H_{04} + H_{24} + H_{26})/hc \right| \nu_2 + \nu_4^{\pm 1}, J, k \pm 3 \right\rangle^{a}_{s} = -\, {}^{a}_{s}\left\langle \nu_2 + \nu_4^{\pm 1}, J, k \pm 3 \left| (H_{04} + H_{24} + H_{26})/hc \right| \nu_2 + \nu_4^{\pm 1}, J, k \right\rangle^{s}_{a} = $$

$$ = -\left\{ \left[\beta^{24} + \beta_J^{24} J(J+1) \right] + \beta_K^{24}\left[k^2 + (k \pm 3)^2 \right] \right\} F_{\pm 3} $$

$$ {}^{s}_{a}\left\langle 3\nu_2, J, k \left| (H_{04} + H_{24} + H_{26})/hc \right| 3\nu_2, J, k \pm 3 \right\rangle^{a}_{s} = -\, {}^{a}_{s}\left\langle 3\nu_2, J, k \pm 3 \left| (H_{04} + H_{24} + H_{26})/hc \right| 3\nu_2, J, k \right\rangle^{s}_{a} = $$

$$ -\left\{ \left[\beta^{222} + \beta_J^{222} J(J+1) \right] + \beta_K^{222}\left[k^2 + (k \pm 3)^2 \right] \right\} F_{\pm 3} $$

$$ {}^{s}_{a}\left\langle \nu_2 + \nu_4^{\pm 1}, J, k \left| (H_{26} + H_{28})/hc \right| \nu_2 + \nu_4^{\pm 1}, J, k \pm 6 \right\rangle^{s}_{a} = \left\{ {}^{(i)}\eta_3^{24} + {}^{(i)}\eta_{3J}^{24} J(J+1) + {}^{(i)}\eta_{3K}^{24}\left[k^2 + (k \pm 6)^2 \right] \right\} F_{\pm 6} $$

$$ {}^{s}_{a}\left\langle 3\nu_2, J, k \left| (H_{26} + H_{28})/hc \right| 3\nu_2, J, k \pm 6 \right\rangle^{s}_{a} = \left\{ {}^{(i)}\eta_3^{222} + {}^{(i)}\eta_{3J}^{222} J(J+1) + {}^{(i)}\eta_{3K}^{222}\left[k^2 + (k \pm 6)^2 \right] \right\} F_{\pm 6} $$

Essential resonances

$$ {}^{s}_{a}\left\langle \nu_2+\nu_4^{\mp1},J,k\pm1\left|\left(H_{22}+H_{24}\right)/hc\right|\nu_2+\nu_4^{\pm1},J,k\right\rangle^{a}_{s}=2\left\{\begin{array}{l}\left[q_{12}+f_{12}^{J}J(J+1)+f_{12}^{JJ}J^2(J+1)^2\right](2k\pm1)+\\ \left[f_{12}^{K}+f_{12}^{JK}J(J+1)\right]\left[k^3+(k\pm1)^3\right]+\\ f_{12}^{KK}\left[k^5+(k\pm1)^5\right]\end{array}\right\}F_{\pm1} $$

$$ {}^{s}_{a}\left\langle \nu_2+\nu_4^{\mp1},J,k\pm1\left|\left(H_{22}+H_{24}\right)/hc\right|\nu_2+\nu_4^{\pm1},J,k\right\rangle^{a}_{s}=-2\left\{q_{12}^{\beta}+f_{12}^{\beta J}J(J+1)+f_{12}^{\beta K}(k^2+(k\pm1)^2)\right\}F_{\pm1} $$

$$ {}^{s}_{a}\left\langle \nu_2+\nu_4^{\mp1},J,k\left|\left(H_{22}+H_{24}\right)/hc\right|\nu_2+\nu_4^{\pm1},J,k\pm2\right\rangle^{s}_{a}=2\left\{\begin{array}{l}{}^{(i)}q_{22}+{}^{(i)}f_{22}^{J}J(J+1)+{}^{(i)}f_{22}^{JJ}J^2(J+1)^2+\\ \left[{}^{(i)}f_{22}^{K}+{}^{(i)}f_{22}^{JK}J(J+1)\right]\left[k^2+(k\pm2)^2\right]+\\ {}^{(i)}f_{22}^{KK}\left[k^4+(k\pm2)^4\right]\end{array}\right\}F_{\pm2} $$

$$ {}^{s}_{a}\left\langle \nu_2+\nu_4^{\mp1},J,k\pm4\left|\left(H_{24}+H_{26}\right)/hc\right|\nu_2+\nu_4^{\pm1},J,k\right\rangle^{s}_{a}=2\left\{\begin{array}{l}{}^{(i)}f_{42}+{}^{(i)}f_{42}^{J}J(J+1)+{}^{(i)}f_{42}^{JJ}J^2(J+1)^2+\\ \left[{}^{(i)}f_{42}^{K}+{}^{(i)}f_{42}^{JK}J(J+1)\right]\left[k^2+(k\pm4)^2\right]+\\ {}^{(i)}f_{42}^{KK}\left[k^4+(k\pm4)^4\right]\end{array}\right\}F_{\pm4} $$

---

[a] $F_{\pm n}=[J(J+1)-k(k\pm1)]^{1/2}[J(J+1)-(k\pm1)(k\pm2)]^{1/2}.....\{J(J+1)-[k\pm(n-1)](k\pm n)\}^{1/2}$;

the (*i*) superscript in the coefficients indicates the parity of the $v_2 = 3$ level involved in the interaction in case of ambiguity.

Acknowledgements

E.C. and F.T. acknowledge the financial support of the University of Bologna (RFO funds). Research described in this paper was partially performed at the Canadian Light Source, which is supported by the Canada Foundation for Innovation, Natural Sciences and Engineering Research Council of Canada, the University of Saskatchewan, the Government of Saskatchewan, Western Economic Diversification Canada, the National Research Council Canada, and the Canadian Institutes of Health Research.

Supplementary material

Supplementary material associated with this article can be found, in the online version, at doi..... .

References

[1] Marty B, Chaussidon M, Wiens RC, Jurewicz AJC, Burnett DS. A N-15-poor isotopic composition for the solar system as shown by genesis solar wind samples. Science 2011;332:1533-6.

[2] Harries D, Hoppe P, Langenhorst F. Reactive ammonia in the solar protoplanetary disk and the origin of Earth's nitrogen. Nat Geosci 2015;8:97-101.

[3] Charnley SB, Rodgers SD. The end of interstellar chemistry as the origin of nitrogen in comets and meteorites. Astrophys J 2002;569:L133-L137. https://doi.org/10.1086/340484.

[4] Lis DC, Wootten A, Gerin M, Roueff E. Nitrogen isotopic fractionation interstellar ammonia. Astrophys J Lett 2010;710:L49-L52. https://doi.org/10.1088/2041-8205/710/1/L49.

[5] Roueff E, Loison JC, Hickson KM. Isotopic fractionation of carbon, deuterium, and nitrogen: a full chemical study. Astron Astrophys 2015;576:A99. https://doi.org/10.1051/0004-6361/201425113.

[6] Wirstrom ES, Charnley SB. Revised models of interstellar nitrogen isotopic fractionation. Monthly Notices Royal Astronomical Society 2018;474:3720-6. https://doi.org/10.1093/mnras/stx3030.

[7] Abbas MM, LeClair A, Owen T, Conrath BJ, Flasar FM, Kunde VG, et al. The nitrogen isotopic ratio in Jupiter's atmosphere from observations by the composite infrared spectrometer on the Cassini Spacecraft. Astrophys J 2004;602:1063-74. https://doi.org/10.1086/381084.

[8] Fletcher LN, Greathouse TK, Orton GS, Irwin PGJ, Mousis O, Sinclair JA, et al. The origin of nitrogen on Jupiter and Saturn from the $^{15}N/^{14}N$ ratio. Icarus 2014;238:170-90. https://doi.org/10.1016/j.icarus.2014.05.007.

[9] Pizzarello S, Williams LB. Ammonia in the early solar system: an account from the carbonaceous meteorites. Astrophys J 2012;749:161. https://doi.org/10.1088/0004-637X/749/2/161.

[10] Mumma MJ, Charnley SB. The chemical composition of comets-emerging taxonomies and natal heritage. In: Faber SM, VanDishoeck E. editors. Annu Rev astron Astrophys, vol. 49, 2011. p. 471-524. https://doi.org/10.1146/annurev-astro-081309-130811.

[11] Bouwman AF, Lee DS, Asman WAH, Dentener FJ, Van Der Hoek KW, Olivier JGJ. A global high resolution emission inventory for ammonia. Global Biogeochemical Cycles 1997;11:561-87. https://doi.org/10.1029/97GB02266.

[12] Adriaenssens S, Staelens J, Wuyts K, van Wittenberghe S, Wuytack T, Verheyen K, et al. Canopy uptake of $^{15}NH_3$ by four temperate tree species and the interaction with leaf properties. Water Air Soil Pollut 2012; 223:5643-57. https://doi.org/10.1007/s11270-012-1304-4.

[13] Felix JD, Elliott EM, Gish T, Maghirang R, Cambal L, Clougherty J. Examining the transport of ammonia emissions across landscapes using nitrogen isotope ratios. Atmospheric Environment 2014;95:563-70. https://doi.org/10.1016/j.atmosenv.2014.06.061.

[14] Ti C, Gao B, Luo Y, Wang X, wang S, Yan X.Isotopic characterization of NHx-N in deposition and major emission sources. Biogeochemistry 2018;138:85-102. https://doi.org/10.1007/s10533-018-0432-3.

[15] Zheng XD,Liu XY, Song W, Sun XC, Liu CQ. Nitrogen isotope variations of ammonium across rain events: implications for different scavenging between ammonia and particulate ammonium. Environmental Pollution 2018;238:392-8. https://doi.org/10.1016/j.envpol.2018.04.015.

[16] Elliott EM, Yu Z, Cole AS, Coughlin JG. Isotopic advances in understanding reactive nitrogen deposition and atmospheric processing. Science of the Total Environment 2019;662:393-403. https://doi.org/10.1016/j.scitotenv.2018.12.177.

[17] Marten A, De Bergh C, Owen T, Gautier D, Maillard JP, Drossart P, et al. Four micron high-resolution spectra of Jupiter in the North Equatorial Belt: H_3^+ emissions and the $^{12}C/^{13}C$ ratio. Planet Space Sci 1994;42:391-9. https://doi.org/10.1016/0032-0633(94)90128-7.

[18] Kleiner I, Tarrago G, Brown LR. Positions and intensities in the $3\nu_2/\nu_2+\nu_4$ vibrational system of $^{14}NH_3$ near 4 μm. J Mol Spectrosc 1995;173:120-45. https://doi.org/10.1006/jmsp.1995.1224.

[19] Cottaz C, Tarrago, G, Kleiner I, Brown LR. Assignments and intensities of $^{14}NH_3$ hot bands in the 5- to 8-μm ($3\nu_2 - \nu_2$, $\nu_2+\nu_4 - \nu_2$) and 4-μm ($4\nu_2 - \nu_2$, $\nu_1 - \nu_2$, $\nu_3 - \nu_2$ and $2\nu_4 - \nu_2$) regions. J Mol Spectrosc 2001;209:30-49. https://doi.org/10.1006/jmsp.2001.8406.

[20] Pearson J, Yu S, Pearson JC, Sung K, Drouin B, Pirali O. Extended measurements and an experimental accuracy effective Hamiltonian model for the $3\nu_2$ and $\nu_2+\nu_4$ states of ammonia. J Mol Spectrosc 2018;353:60-6. https://doi.org/10.1016/j.jms.2018.09.004.

[21] Pearson JC, Yu S, Pirali O. Modeling the spectrum of the $2\nu_2$ and ν_4 states of ammonia at experimental accuracy. J Chem Phys 2016;145:124301-13. https://doi.org/10.1063/1.4961656.

[22] Down MJ, Hill C, Yurchenko SN, Tennyson J, Brown LR, Kleiner I. Re-analysis of ammonia spectra: Updating the HITRAN $^{14}NH_3$ database. J Quant Spectrosc Radiat Transfer 2013;130:260-72. https://doi.org/10.1016/j.jqsrt.2013.05.027.

[23] Di Lonardo G, Fusina L, Trombetti A, Mills IA. The ν_2, $2\nu_2$, $2\nu_2$, ν_4 and $\nu_2+\nu_4$ bands of $^{15}NH_3$. J Mol Spectrosc 1982;92:298-325.

[24] Urban Š, Špirko V. Papoušek D, McDowell RS, Nereson NG, Belov SP, et al. Coriolis and *l*-type interactions in the ν_2, $2\nu_2$ and ν_4 states of $^{14}NH_3$. J Mol Spectrosc 1980;79:455-95.

[25] Fusina L, Di Lonardo G, Canè E, Predoi-Cross A, Rozario H, Herman M. The high resolution spectrum of $^{15}NH_3$ in the far-infrared: Rotation-inversion transitions in the ground, $\nu_2 = 1,2$ and $\nu_4 = 1$ states. J Quant Spectrosc Radiat Transfer 2017;203:417-24. https://doi.org/10.1016/j.jqsrt.2017.01.021.

[26] Yurchenko SN. A theoretical room-temperature line list for $^{15}NH_3$. J Quant Spectrosc Radiat Transfer 2015;152:28-36. https://doi.org/10.1016/j.jqsrt.2014.10.023.

[27] Canè E, Di Lonardo G, Fusina L, Tamassia F, Predoi-Cross A. The $\nu_2 = 1$, 2 and $\nu_4 = 1$ bending states of $^{15}NH_3$ and their analysis at experimental accuracy. J Chem Phys 2019;150:194301. https://doi.org/10.1063/1.5088751.

[28] Gordon IE, Rothman LS, Hill C, Kochanov RV, Tan Y, Bernath PF, et al. The HITRAN 2016 molecular spectroscopy database. J Quant Spectrosc Radiat Transfer 2017;**203**: 3-69. https://doi.org/10.1016/j.jqsrt.2017.06.038.

[29] Sarka K, Schrötter HW. Effective Hamiltonian for rotation-inversion states of ammonia–like molecules. J Mol Spectrosc 1996;179:195-204. https://doi.org/10.1006/jmsp.1996.0197.

[30] Aliev MR, Watson JKG. Calculated sextic centrifugal distortion constants of polyatomic molecules. J Mol Spectrosc 1976;61:29-52.

Figure Captions

Fig. 1. The FTIR spectrum of the $3\nu_2$ and $\nu_2+\nu_4$ bands for $^{15}NH_3$. The band centers are indicated. Experimental conditions: pressure 267 Pa; path-length 6 m.

Fig. 2. The $^{q}P_K(8)$ and $^{q}P_K(7)$ sub-branches in the $s \leftarrow a$ $3\nu_2$ cold band of $^{15}NH_3$ .The K assignments are indicated. Experimental conditions: pressure 267 Pa; path-length 6 m.

Fig. 3. The $^{p}P_K(9)$ sub-branch in the $s \leftarrow s$ $\nu_2 + \nu_4$ cold band of $^{15}NH_3$ .The K assignments are indicated. Experimental conditions: pressure 267 Pa; path-length 6 m.

Fig. 4. Energy diagram of $^{15}NH_3$ showing the GS and the levels located from 750 to 3000 cm^{-1}. The experimental term values are given in cm^{-1}. The types of the assigned transitions are highlighted. The vibration-rotation-inversion transitions are indicated by black and red arrows, for the cold and hot bands, respectively. The rotation-inversion and pure inversion transitions are indicated by blue arrows.

Figure 1

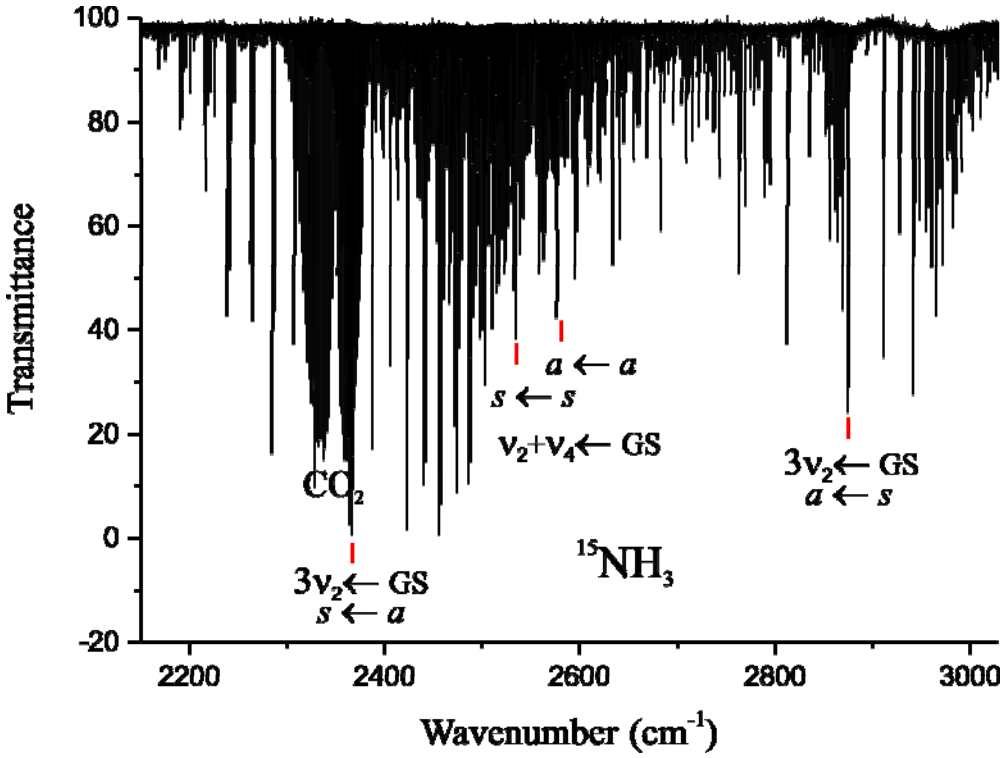

Figure 2

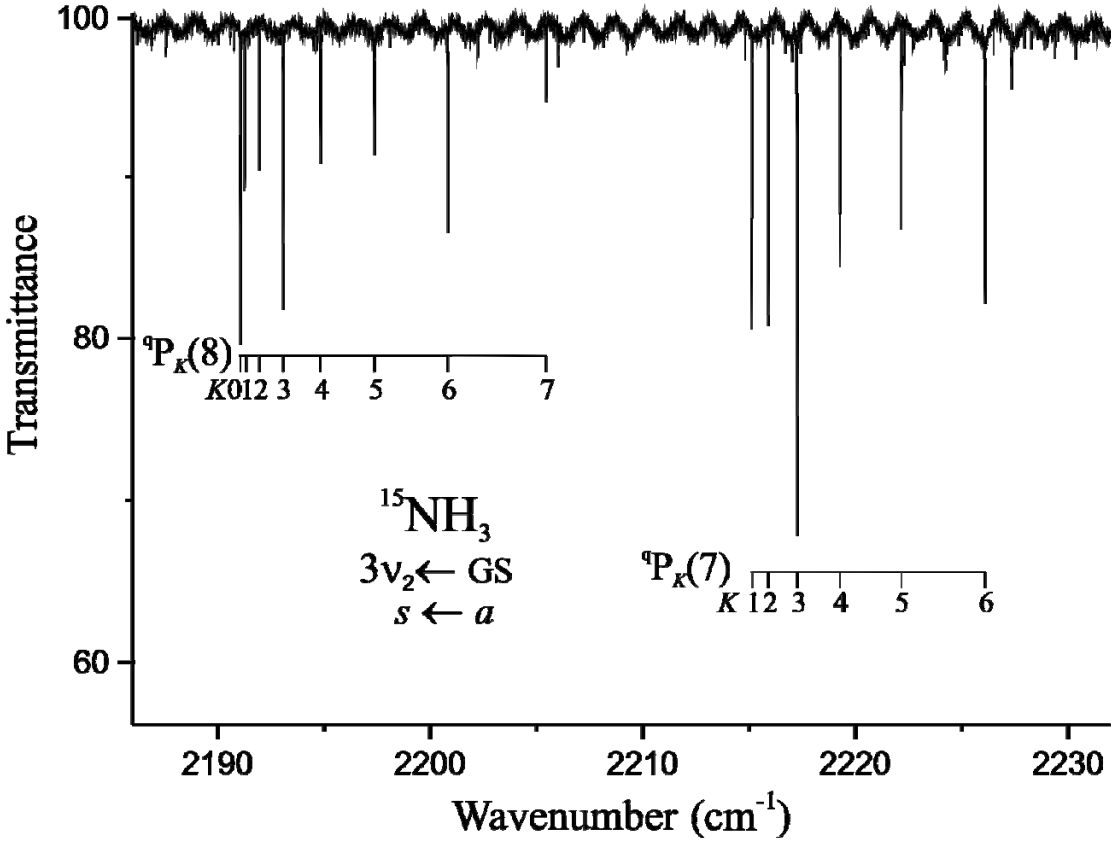

Figure 3

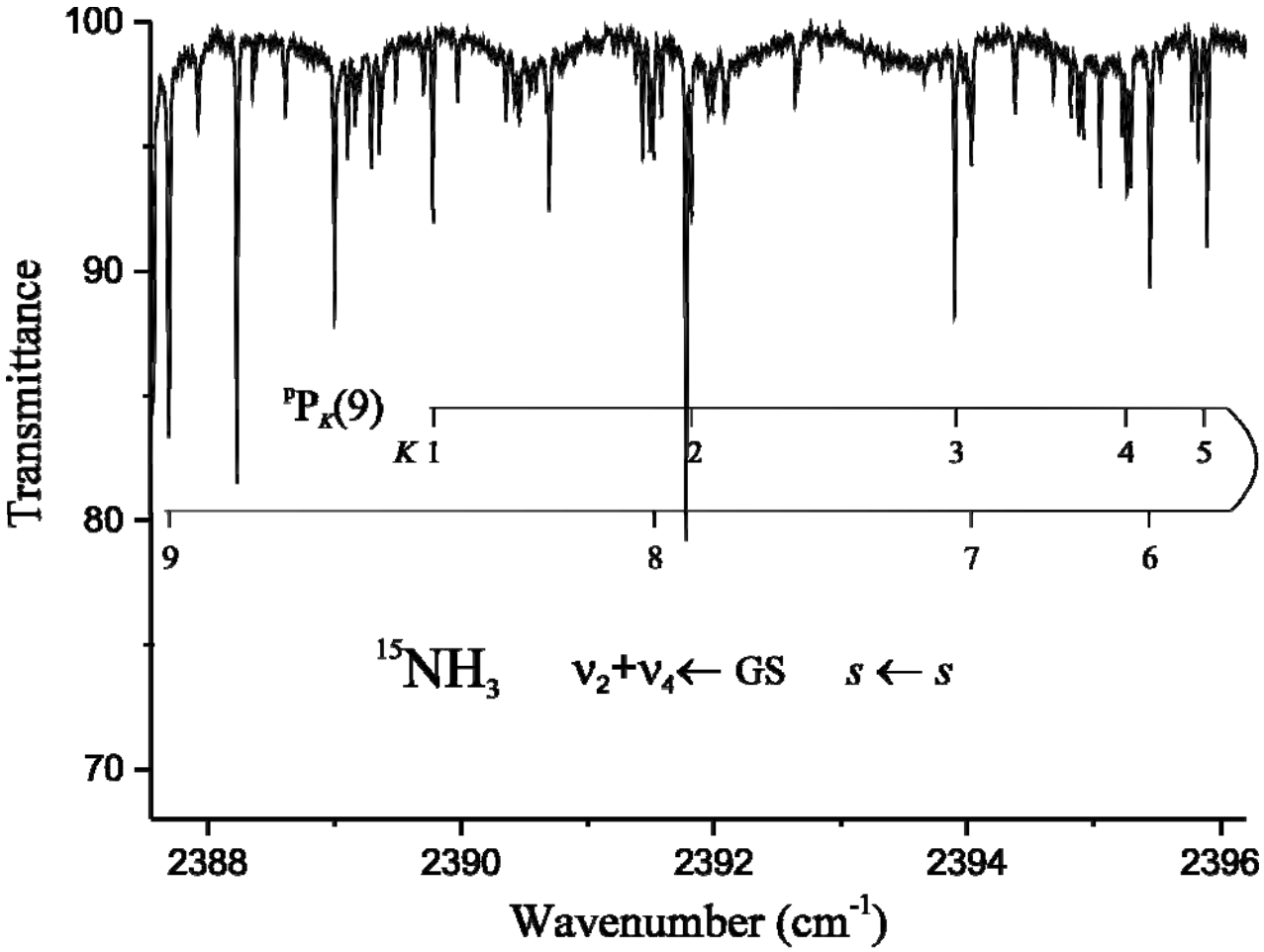
100
90
80
70
Transmittance
$^{P}P_{K}(9)$
K 1
2
3
4
5
9
8
7
6
$^{15}NH_3$ $\nu_2+\nu_4 \leftarrow$ GS $s \leftarrow s$
2388
2390
2392
2394
2396
Wavenumber (cm^{-1})

Figure 4

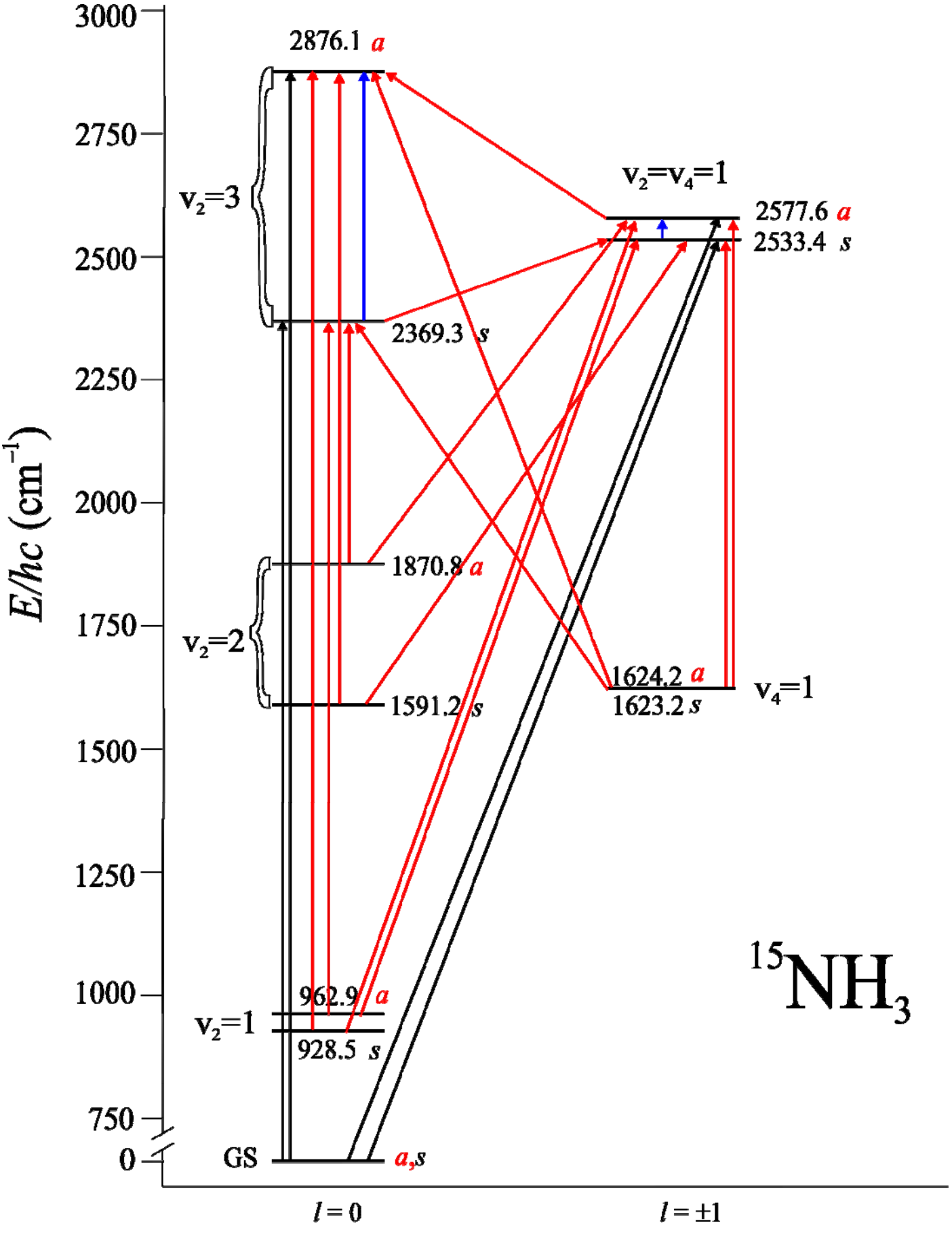
3000
2750
2500
2250
2000
1750
1500
1250
1000
750
0
E/hc (cm-1)
2876.1 a
v2=3
2369.3 s
v2=v4=1
2577.6 a
2533.4 s
1870.8 a
v2=2
1591.2 s
1624.2 a
1623.2 s
v4=1
962.9 a
v2=1
928.5 s
GS
a,s
15NH3
l = 0
l = ±1